Time-domain optical coherence tomography with digital holographic microscopy

Pia Massatsch, Florian Charrière, Etienne Cuche, Pierre Marquet, and Christian D. Depeursinge

We show that digital holography can be combined easily with optical coherence tomography approach. Varying the reference path length is the means used to acquire a series of holograms at different depths, providing after reconstruction images of slices at different depths in the specimen thanks to the short-coherence length of light source. A metallic object, covered by a 150-μm-thick onion cell, is imaged with high resolution. Applications in ophthalmology are shown: structures of the anterior eye, the cornea, and the iris, are studied on enucleated porcine eyes. Tomographic images of the iris border close to the pupil were obtained 165 μm underneath the eye surface.

OCIS codes: 090.0090, 090.1760, 110.4500, 170.7050.

1. Introduction

Modern medicine and therapy rely on early and precise diagnosis to permit localized and specific treatments to be used with optimum outcomes. In particular, imaging the various epithelia at the surface of organs inside or outside the body is of particular importance for the early detection of dysfunction and lesions. Three-dimensional (3D) imaging of complex microscopic and submicroscopic processes in tissues, down to the cellular level, is still a challenging issue. Rapid, sensitive, noninvasive methods with high-resolution capability are thus needed for diagnosis of lesions or tissue dysfunctions. Digital holographic microscopy (DHM) offers new opportunities likely to fulfill these requirements.

Optical coherence tomography (OCT) still seems the most popular imaging method capable of giving cross-sectional views of a 3D semitransparent object.[1,2] It has been used extensively to image tissues in a depth reaching 2 mm. A plurality of clinical applications has been developed. The first clinical application and nowadays the most important one is ophthalmology, in which detailed views of the different parts of the eye, the retina in particular, can be obtained. OCT also finds applications in the observation of different mucosa, such as in the esophagus and of the skin. It is based on the measurement of the interference between the incident ray reflected by the object and a reference beam reflected by a moving mirror. Reducing the coherence length of the irradiating beam brings discrimination in depth. Basically, this technique measures the reflected signal at a single point of the scattering object, and one can obtain an image along a line by sliding the reference mirror on a distance equivalent to the desired depth of the image. Full 3D image of the scattering object is finally obtained by additional scanning of the object in the transverse directions. The traditional approach insures a high sensitivity and a large dynamic range, but limited lateral resolution, because the numerical aperture (NA) of the focusing lens must be kept low to preserve the depth of focus, and special arrangements with adaptive focusing may allow the use of higher NA objectives. As a result of a compromise between decreased lateral resolution and improved axial resolution, cellular structures could be observed with the so-called ultra-high-resolution OCT.[3] High spatial coherence of the emitting source combined with a low temporal coherence could be achieved by using ultrashort laser pulses (<50 fs). Various imaging modalities have been proposed to yield tomographic images: the early studies and now most of the instruments present cross-sectional images, i.e., im-

At the time this research was performed, P. Massatsch, F. Charrière (florian.charriere@epfl.ch), E. Cuche, and C. D. Depeursinge were with the Imaging and Applied Optics Institute, Polytechnique Fédérale de Lausanne EPFL, BM4.142, 1015 Lausanne, Switzerland. E. Cuche is now with Lyncée Tec SA, rue du Bugnon 7, CH-1005 Lausanne, Switzerland. P. Marquet is with the Physiology Institute, rue du Bugnon 7, CH-1005 Lausanne, Switzerland.

Received 22 July 2004; revised manuscript received 25 November 2004; accepted 30 November 2004.

0003-6935/05/101806-07$15.00/0

ages in the x–z plane, containing the axis of the beam propagation. However, other modalities have been proposed[4]: *en face* tomographic images show images along the x–y plane, i.e., in the plane normal to the beam propagation. As possible drawbacks of the scanning approach in time-domain OCT, its potential slowness and sensitivity to motion artifacts should be mentioned. For that reason, the concept of parallel OCT was proposed.[5] It consists of multiplying the number of scanned lines by making them work in parallel. Ensuring low crosstalk between the channels requires the design of a matrix of uncorrelated and low-coherence emitters. The realization requires also an important amount of energy to provide sufficient emitter power. Recently, it was established by Dubois *et al.*[6] that ultra-high-resolution (1.8 μm × 0.9 μm for transverse x axial resolution), full-field OCT can be achieved with a white-light thermal source. High transverse resolution can be achieved thanks to a relatively high NA microscope objective (NA = 0.3). The Linnik configuration is used, and careful adjustment of the wave fronts is necessary for direct viewing of the sample.[7,8] A drawback of the bright-field approach is its limited dynamic range (<90 dB), owing to a large amount of parasitic light that originates from multiple scattered photons and that may blind the camera. This fact significantly restricts the observation depth. Because of the limited depth of focus in this optical arrangement, another possible drawback is the necessity to move the sample along the z axis. Practically, this feature restricts the use of the method to *in vitro* applications.

DHM offers another perspective by providing an enlarged depth of focus, without compromise of the high NA of the microscope objective required for good lateral resolution. This large depth of focus is provided by the possibility of numerically reconstructing the image of the object at a variable reconstruction distance, which is considered a freely adjustable parameter in the numerical reconstruction process. DHM is of particular interest from the point of view of its robustness and flexibility. One particular feature of digital holography makes it possible, in theory, to catch all the 3D configuration of the scattering object on a single hologram. This basic feature of holography is exploited in the so-called in-line holography, where the 3D arrangements of isolated scattering centers are computed from a single hologram. Nevertheless, the hypothesis of the validity of the first Born approximation, i.e., that each photon is diffracted only once in the sample without multiple diffraction, which is at the basis of the in-line holographic approach, is usually not met in dense scattering media such as biological tissues, and multiple scattered photons introduce an excessive speckle or background noise in the reconstruction process. Coherence gating can be introduced in the hologram generation process to eliminate part of the undesirable contribution to the hologram, mainly originating from scatterers outside the region of interest. Short-coherence holography developed with photorefractive media (multiquantum wells) was proposed in 1995

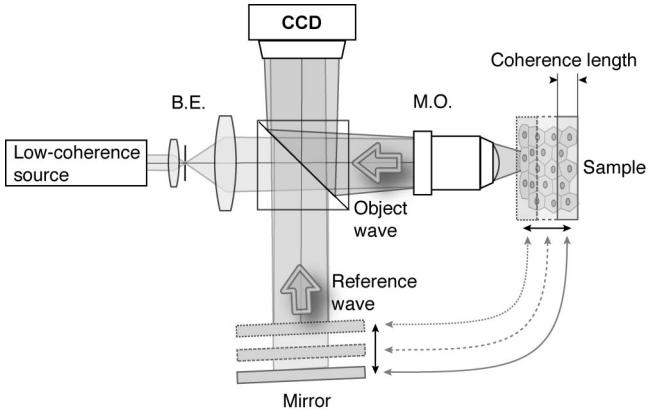

Fig. 1. Sketch of the optical system used to achieve OCT with a short-coherence digital holographic microscope. B.E., beam expander; M.O., microscope objective.

(Hyde *et al.*[9]) to isolate surfaces or slices in the reconstruction process that was performed optically in this case.[10] In 1997, Cuche *et al.*[11] proposed to combine short-coherence and DHM technology to create a new tomographic modality. In 2000, Indebetouw and Klysubun[12] proposed a method of imaging through scattering media with depth resolution by use of low-coherence gating in spatiotemporal digital holography. The source is an extended white-light source. However, the optical arrangement limits severely the possibility of using a high NA microscope objective, and the lateral resolution is insufficient to observe cells. In the following two years, two papers were published on the use of short coherence in digital holography.[13,14] Researchers report the use of lensless instruments and generally describe them as superior because of the absence of aberrations introduced by the lenses and of the broad spectrum available for imaging. However, there are several important advantages to using lenses or microscope objectives: in lensless systems, the NA is limited by the optical setup, encompassing the sample, the CCD chip, and the mirror or beam-splitter cube needed for beam recombination. NAs of approximately 0.2 are achieved experimentally. Such achievement means that important losses of the high spatial frequency components must be conceded and that observation of fine cellular structures cannot be recorded with such devices. The holographic method developed here rests on the use of microscope objectives, and very high NAs higher than 1 are possible. Small details can therefore be observed, in particular the cellular structure of epithelia. DHM with short-coherence sources therefore seems a possible alternative to current time-domain OCT.

2. Basic Principle of Optical Coherence Tomography with Digital Holographic Microscopy

A hologram results from the interferences between an object wave being scattered by a sample and a reference wave. Figure 1 shows the principle of OCT with DHM. The configuration is basically that of a

Michelson interferometer. A hologram is formed by the interference of a beam diffracted by a volume object and a reference wave reflected by a moving tilted mirror. In this way not only the amplitude but also the phase distribution of the object wave is encoded. When the hologram is reilluminated by a digital replica of the reference wave, the original object wave front is reconstructed digitally.

In digital holography the hologram is recorded on a charge-coupled device (CCD) camera and reconstructed numerically on a personal computer, giving direct access to the phase and amplitude of the reconstructed wave front. The method has been adapted to microscopy and a new imaging technique called DHM was born.[15–18] This technique has been applied for biological cells investigation. With a Pentium 4 2.8 Ghz, 3D phase reconstructions of 512 $\times$ 512 pixels have already been achieved at a rate of 15 frames/s.

When this technique is combined with the use of light with low temporal coherence, it is possible to perform optical tomography of the specimen. A series of holograms resulting from the interference of the reference beam and the light diffracted at different depths in the specimen are formed, and each of these holograms provide, after wave-front reconstruction, cumulated phase and amplitude data along the optical path, yielding a detailed tomographic image of the object. The thickness of a tomographic layer is half of the coherence length of the light source in the medium owing to the reflection setup, which is basically the axial resolution of the system. With a coherence length of 24 μm, the axial resolution is supposed to be 12 μm in air; an experimental measurement gave a value of 11 μm. The reconstructed image can be calculated anywhere in the coherence length thanks to the digital focusing capability of DHM (see Section 4 for details on the reconstruction process). In the research presented here, all the images are calculated at the center of the coherence length in the sample where the intensity is maximum, but as in classical microscopy, the reconstructed images contain blurred information from the planes out of the focus plane that are still in the coherence length but at a sensibly lower intensity compared with the in-focus information.

3. Experimental Setup

The holograms were recorded with an off-axis experimental configuration, similar to the digital holographic reflection microscope described by Cuche *et al.*,[18] which scheme is summed up in Fig. 1. The microscope was designed to image horizontal objects, in particular biological samples. The microscope objective has a magnification of 10$\times$ and a NA of 0.35. The low-coherence source is a linearly polarized Ti: sapphire laser (Coherent Model MIRA-900) operated at a wavelength of 800 nm and producing 80-fs pulses, corresponding to a coherence length of 24 μm in air. A neutral density filter was used for the adjustment of the intensities in the reference arm and the object arm of the interferometer. One or two beam expanders, including pinholes for spatial filtering, are introduced in the arms of the interferometer to produce clean plane waves. The sample is illuminated through the microscope objective with a collimated beam. A variable delay could be introduced between the object wave and the reference wave so that sliding the coherent gate allows scanning of the sample in depth. The hologram detection was achieved by a standard 512 $\times$ 512 black and white CCD camera with a lens-on-chip configuration that renders approximately the entire detector area light sensitive. The pixel size was 11 μm $\times$ 11 μm. A frame-grabber board installed on the computer was used to perform hologram digitalization. A signal-to-noise ratio (SNR) of 60 dB is achieved with the CCD for the hologram acquisition.

4. Reconstruction Process

The reconstruction process and the method of adjusting the reconstruction parameters have been described by Cuche *et al.*[17,18] It consists of simulating the standard optical reconstruction of the digitized hologram with purely numerical steps. The intensity on the hologram is given by

$$I_H(x,\ y) = \underbrace{\mathbf{OO}^* + \mathbf{RR}^*}_{\text{zero order}} + \underbrace{\mathbf{O}^*\mathbf{R}}_{\text{real image}} + \underbrace{\mathbf{RO}^*}_{\text{virtual image}}, \quad (1)$$

where **O** and **R** are the object and the reference fields impinging on the hologram respectively. A digital hologram is recorded by a black-and-white CCD camera and transmitted to a computer. The digital hologram $I_H(k, l)$ is an array of $N \times N$ (usually 512 $\times$ 512 or 1024 $\times$ 1024), 8-bit-encoded numbers resulting from the two-dimensional sampling of $I_H(x, y)$ by the CCD camera,

$$I_H(k,\ l) = \int_{k\Delta x - \Delta x/2}^{k\Delta x + \Delta x/2} \int_{l\Delta y - \Delta y/2}^{l\Delta y + \Delta y/2} I_H(x,\ y)\mathrm{d}x\mathrm{d}y, \quad (2)$$

where k, l are integers and Δx, , Δy define the sampling intervals in the hologram plane (pixel size). Classically, the reconstruction is achieved by illumination of the hologram with a replica of the reference wave, generating a transmitted wave front $\Psi = \mathbf{R}I_H$. This field propagates toward an observation plane, where a 3D image of the object can be observed. Here, taking advantage of the digital recording of the hologram, the transmitted wave front $\Psi(\xi, \eta)$ is simulated by multiplication of the hologram intensity distribution $I_H(k, l)$ by a so-called digital reference wave $\mathbf{R_D}(k, l)$. Assuming that a plane wave is used as reference, the digital reference wave $\mathbf{R_D}$ is defined

$$\mathbf{R_D}(k,\ l) = \exp[i(k_x\, k\Delta x + k_y\, l\Delta y)], \quad (3)$$

where k_x, k_y are two phase reconstruction parameters, which must be adjusted to match as closely as possible the propagation direction of the experimen-

tal reference waves $\mathbf{R}$. The computed wave front Ψ is now defined in the hologram plane xy and can be evaluated at any distance from hologram plane by a numerical calculation of the scalar diffraction in the Fresnel approximation. The reconstructed wave front $\Psi(\xi, \eta)$, at a distance d from the hologram plane, in an observation plane $\xi\eta$, is computed by use of a discrete expression of the Fresnel integral

$$\Psi(m,\ n) = A\Phi(m,\ n)\exp\left[\frac{i\pi}{\lambda d}\,(m^2\Delta\xi^2 + n^2\Delta\eta^2)\right] \times \mathrm{FFT}\left\{\mathbf{R_D}(k,\ l)I_H(k,\ l)\exp\left[\frac{i\pi}{\lambda d}(k^2\Delta x^2 + l^2\Delta\eta^2)\right]\right\}_{m,\,n}, \tag{4}$$

where m and n are integers ($-N/2 \le m, n < N/2$), FFT is the fast Fourier transform operator, $A = \exp(i2\pi d/\lambda)/(i\lambda d)$, and $\Phi(m, n) = \exp[(-i\pi/\lambda)(m^2\Delta\xi^2/d\xi + n^2\Delta\eta^2/d\eta)$ is the so-called digital phase mask with parameters $d\xi$ and $d\eta$ digitally adjusted to correct the phase aberration due to the microscope objective. $\Delta\xi$ and $\Delta\eta$ are the sampling intervals in the observation plane.

Considering only the virtual images of Eq. (1), the propagated wave front corresponding to the computed digital reference wave is

$$\Psi = \mathbf{R_D}\mathbf{R}^*\mathbf{O}, \qquad \text{with } \mathbf{R_D}(k,\ l) = \exp[i(k_x\, k\Delta x + k_y\, l\Delta y)], \tag{5}$$

where k_x and k_y are two parameters adjusted to achieve identical propagation directions for $\mathbf{R}$ and $\mathbf{R_D}$. The off-axis geometry allows separation of the different diffraction orders, so the area corresponding to Ψ can be selected in the reconstruction plane. The useful part of the spectrum used for the reconstruction is only a fourth of the hologram spectrum, what corresponds to a loss of a factor 2 in the resolution if we compare the reconstructed image with a standard focal plane image.

5. Demonstration of the Principle of Short-Coherence Digital Holographic Microscopy: Vision through an Onion Cell Layer

Performing tomography by short-coherence DHM for layers hidden behind biological structures is demonstrated. A reflecting 1951 USAF glass slide resolution target is hidden behind a monocellular onion membrane, and holograms are recorded at the surface and at the level of the USAF test target [Fig. 2(a)].

The amplitude reconstruction of holograms recorded with the coherent gate at the surface and at the level of the USAF test target are presented in Fig. 2. Effects of hologram filtering are present in the lower left corner of the images. A cell pattern corresponding to the reflection of the membrane is visible in the amplitude image [Fig. 2(b)]. In the amplitude reconstruction of the USAF test target, [Fig. 2(c)], located 150 μm below the surface of the onion membrane, the element number "2" of group 3 is clearly visible, covered by the shadow of the onion layer similar to the reflected amplitude in Fig. 2(b). It is thus possible to image an object hidden behind a complex biological structure.

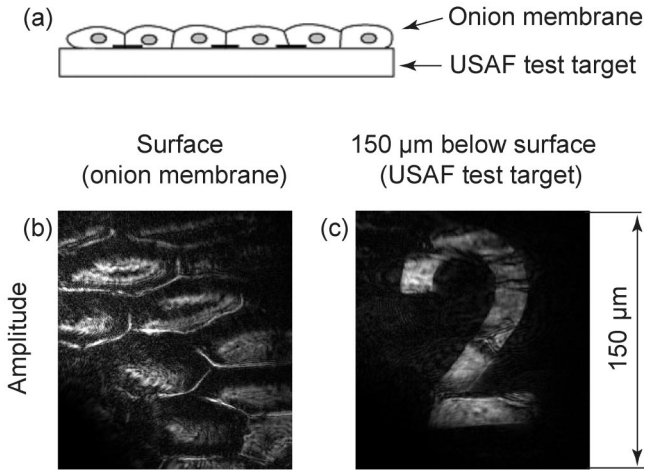

Fig. 2. *En face* tomographic images of the complex object composed of a USAF test target (part of it containing the number "2") covered by an onion cell layer. These images have been obtained by the reconstructions of holograms taken with coherence gates at the level of the surface of the onion cells and at the level of the USAF test target. (a) Sketch of the sample. (b) *En face* image from the hologram taken with the coherence gate at the surface. (c) *En face* image from the hologram recorded 150 μm below the surface, at the level of the USAF test target.

6. Application of Short-Coherence Digital Holographic Microscopy to Obtain Tomographic Images of a Biological Sample: a Porcine Eye

Several experiments were performed in the attempt to image the structures in the anterior part of enucleated porcine eyes; 3D tomography of the cornea and of the border of the iris close to the pupil are presented. Schematic images of the eye and the cornea are shown in Figs. 3(a) and 3(b). The anterior part of the eye contains the following structures to be imaged: the cornea, the iris, and the lens. The first layer of the cornea consists of a transparent epithelium formed by a multiply layered stack of living cells with a nucleus and cytoplasm.

The main structures of the 550-μm-thick cornea are the epithelium, the stroma, and the endothelium. The epithelium is the 40-μm-thick external cell layer of the cornea. New epithelial cells are continuously growing on the stromal side, and old cells are evacuated by the blinking movements of the eyelid. The stroma is the relatively homogenous bulk structure in the middle of the cornea, separated from the epithelium by Bowman's membrane and from the endothelium by Descemets's membrane. The endothelium is the 10-μm-thick monocellular layer lining the interior of the cornea. The endothelium is a nonregenerative tissue, and the observation of the size and the shape of endothelial cells provides important infor-

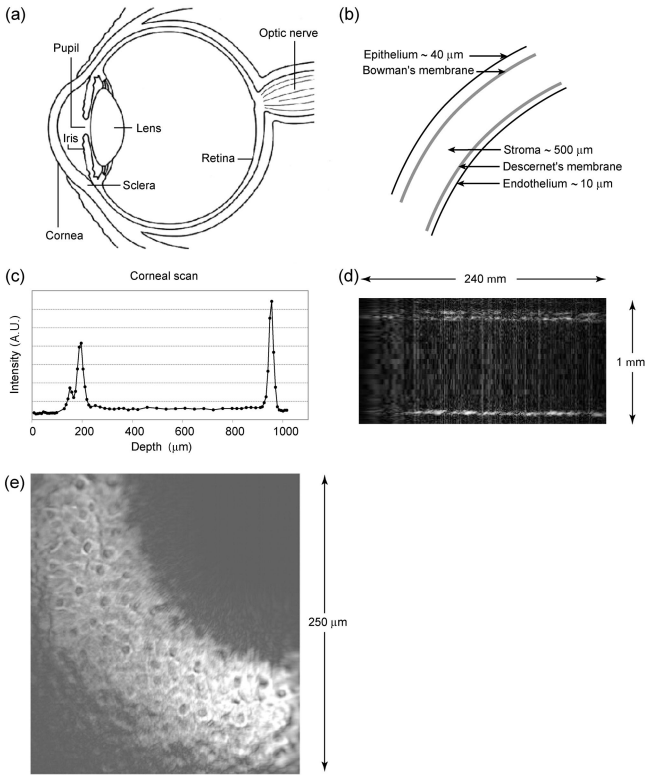

Fig. 3. Sketches representing (a) the eye and (b) the cornea with its fine structure. (c) Backscattered intensity, obtained by scanning through the cornea. The double peak corresponds to the thick epithelium. The single peak to the right corresponds the endothelial monocellular layer. (d) Cross-sectional image of the whole cornea. The two interfaces of the epithelium are visible at the top of the image, and the endothelial layer is visible at the bottom. (e) *En face* image of porcine corneal epithelium *in situ*. This tomographic image yields details at the cellular level: image of nuclei and cytoplasm. (The upper right and the lower left parts of the image contain no information because of the convex form of the cornea).

mation on the condition of the eye. A tear film covers the cornea. It has a layered structure with a lipid component "floating" as a 100-nm-thin oil layer on the surface, over a 6–10-μm-thick aqueous layer. Under this tear film cover, a mucin layer is adjacent and adherent to the corneal epithelial surface. Note that Bowman's membrane is absent in porcine eyes, used in our experiments. The porcine cornea and epithelium are also thicker than the corresponding human tissues, 700–800 μm for the cornea and 50–60 μm for the epithelium, whereas the endothelium seems to be slightly thinner, approximately 6 μm.[19]

7. Cross-Sectional and En Face Tomography of the Cornea of a Porcine Eye

To be able to penetrate far enough into the eye and extract information from the entire thickness of the cornea, immersion of the eye in a physiological solution (0.9% NaCl water solution) was performed and the microscope objective placed in the solution. A stack of holograms was recorded on the cornea of a freshly enucleated porcine eye. Holograms were recorded every 8 μm in the region of the epithelium and endothelium and every 40 μm in the middle of the stroma. The graph in Fig. 3(c) shows the backscattered signal throughout the whole thickness of the cornea. Each point was obtained by calculation of the average intensity over an area of $10 \times 10\ \mu m^2$ in the reconstructed image plane, normal to the scanning direction. The double peak to the left corresponds to the relatively thick epithelium and the peak to the right to the thin monocellular endothelial layer. The thickness of the epithelium was estimated to be 50 μm and the thickness of the cornea to approximately 800 μm. These values match well the thickness of the porcine cornea measured by other methods.[19] An estimation of the endothelial thickness was not possible because this layer is thinner than the depth resolution of the method.

The cross-sectional image of the section in the cornea is presented in Fig. 3(d). The axial resolution of this image is defined by the depth resolution of short-coherence DHM (approximately 11 μm). The pixel size is set to 8 μm, the minimal step length used during recording. The holographic setup determines the resolution in the plane of the cornea section: approximately 1 μm for the characteristics of the microscope objective used in these measurements. Experimentally, this resolution, which is close to the diffraction limit, could be verified. A pixel size of 1 μm was retained in agreement with the resolution of DHM, and the resolution was proved sufficient to observe subcellular details of the epithelial layer inside the 40-μm-thick layer [Fig. 3(e)]. The main reflective layers appear slightly tilted relative to the optical axis (y axis in the image). This tilt is due to the use of low-coherence light in combination with the off-axis geometry of the holographic setup (beam walk-off), because the fringes on the hologram originate from different depths in the object. The reconstructed image then corresponds to an oblique object slice slightly tilted at an angle in relation to a plane perpendicular to the illumination.

8. Cross-Sectional and En Face Tomography of the Iris of a Porcine Eye

Imaging of the iris was motivated not only by the interest of monitoring this structure but also for illustrating the performances of short-coherence DHM to image biological structures in a highly scattering translucent media.

Tomography of the porcine iris was performed at the pupil border of a freshly enucleated porcine eye immersed in water. A stack of holograms was recorded, and a 3D reconstruction of the iris was performed slice by slice. The voxel size is 1 μm in the x–y directions, whereas the voxel size in the z direction, determined by the path-length difference of the reference wave between two consecutive holograms in the stack, is 4 μm. Several planes in the reconstructed volume are presented in Fig. 4. Figure 4(i) is the *en face* view given by the amplitude reconstruction, 50 μm beneath the iris surface; the inhomoge-

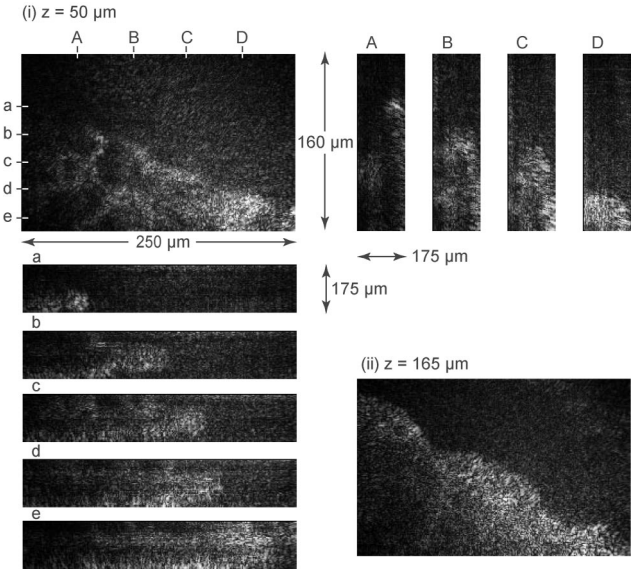

Fig. 4. Tomographic images of the porcine iris, at the pupil border. Image (i) is the *en face* image taken 50 μm underneath the iris surface. Image (ii) is the *en face* image taken 165 μm underneath the surface. Images a–e and A–D represent cross-sectional images taken through the iris at locations given by the letters sketched in image (i). The anterior part of the iris is at the top for images a–e and to the left for images A–D.

neous character of the iris tissue is observed. Figure 4(ii) is *en face* view given by the amplitude reconstruction, 165 μm beneath the surface; we can observe that the tissue is more uniform at this depth. In Fig. 4(i), both sets of a–e and A–D show cross-sectional sections through the iris. The round border of the iris is visible as well as the inhomogeneities at the iris surface. It should be stressed that the voxel size of these cross-sectional views is not square. They measure 1 μm × 4 μm, although they have quadratic representation in the illustrations. These results are promising even though imaging at the cellular level is not possible with the present depth resolution. Larger structures can be observed, and the penetration into the iris tissue is good. A potential application is to study the zonular apparatus, hidden behind the iris, with a setup adapted to the dimensions and the location of these structures. The zonular fibers and the ciliary body play an important role in visual accommodation, and high-resolution ultrasound biomicroscopy has already been used to image these structures *in vivo*,[20] but at a lower lateral resolution.

9. Discussion and Conclusion

The objective of this study, which was to demonstrate the feasibility of performing tomography of biological material with short-coherence digital holographic microscopy, can be considered met: First, it has been shown that observation of scattering objects (part of USAF test target) imbedded in biological material, such as onion cells, is possible with a high transversal resolution, since the system is simply diffraction limited. It was also demonstrated that imaging different structures in the eye, such as the cornea epithelium and the iris, could be carried out successfully. It was also shown, for the first time to our knowledge with short-coherence DHM that details could be obtained at the subcellular level on the image of cornea epithelium. The lateral resolution is similar to that obtained by Dubois *et al.*[6] with full-field OCT, but the axial resolution is worse (11 μm). This worsening is due to the bandwidth of the source, which is only 15 nm in our short-coherence DHM setup and must be compared with the several hundreds of nanometers for a white-light source. This quantity could also be much improved in holography by use of sources with a broader bandwidth, but a minimal bandwidth must be fixed to preserve the formation of the hologram, i.e., because of the of axis configuration, the coherence length must be sufficient to allow interference fringes formation over the entire chip of the camera. This necessity is the main drawback to axial resolution. However, the resolution of short-coherence DHM is better than the resolution of ultrasound (35 μm axial),[21] and complementary information might be obtained. Many studies still need to be conducted to improve the significance of the detected signal. In particular, the phase information, which results from the numerical reconstruction in digital holography, is not used in the present study. Its potential interest is great, however, and should be taken into account in the evaluation of the role of the refractive index of tissues along the optical path length. DHM is also of prime interest in measurement in both the study and the imaging of biological and turbid media.

This research has been supported by the Swiss National Science Foundation (SNSF) grants 21-67068.01 and 205320-103885/1.

References

1. D. Huang, E. A. Swanson, C. P. Lin, J. S. Schuman, W. G. Stinson, W. Chang, M. R. Hee, T. Flotte, K. Gregory, C. A. Puliafito, and J. G. Fujimoto, "Optical coherence tomography," Science **254,** 1178–1181 (1991).
2. A. F. Fercher, "Optical coherence tomography," J. Biomed. **1,** 157–173 (1996).
3. W. Drexler, "Ultrahigh resolution optical coherence tomography," J. Biomed. Opt. **9,** 47–74 (2004).
4. A. G. Podoleanu, J. A. Rogers, and D. A. Jackson, "OCT *en-face* images from the retina with adjustable depth resolution in real time," IEEE J. Sel. Topics Quantum Electron. **5,** 1176–1184 (1999).
5. S. Bourquin, V. Monterosso, P. Seitz, and R. P. Salathe, "Video-rate optical low-coherence reflectometry based on a linear smart detector array," Opt. Lett. **25,** 102–104 (2000).
6. A. Dubois, K. Grieve, G. Moneron, R. Lecaque, L. Vabre, and C. Boccara, "Ultrahigh-resolution full-field optical coherence tomography," Appl. Opt. **43,** 2874–2883 (2004).
7. L. Vabre, A. Dubois, and A. C. Boccara, "Thermal-light full-field optical coherence tomography," Opt. Lett. **27,** 530–532 (2002).
8. A. Dubois, L. Vabre, A. C. Boccara, and E. Beaurepaire, "High-resolution full-field optical coherence tomography with a Linnik microscope," Appl. Opt. **41,** 805–812 (2002).
9. S. C. W. Hyde, N. P. Barry, R. Jones, J. C. Dainty, P. M. W. French, M. B. Klein, and B. A. Wechsler, "Depth-resolved ho-

lographic imaging through scattering media by photorefraction," Opt. Lett. **20,** 1331–1333 (1995).
10. M. Tziraki, R. Jones, P. M. W. French, D. D. Nolte, and M. R. Melloch, "Short-coherence photorefractive holography in multiple-quantum-well devices using light-emitting diodes," Appl. Phys. Lett. **75,** 1363–1365 (1999).
11. E. Cuche, P. Poscio, and C. Depeursinge, "Optical tomography by means of a numerical low-coherence holographic technique," Journal of Optics-Nouvelle Revue D'Optique **28,** 260–264 (1997).
12. G. Indebetouw and P. Klysubun, "Imaging through scattering media with depth resolution by use of low-coherence gating in spatiotemporal digital holography," Opt. Lett. **25,** 212–214 (2000).
13. G. Pedrini and S. Schedin, "Short coherence digital holography for 3D microscopy," Optik **112,** 427–432 (2001).
14. G. Pedrini and H. J. Tiziani, "Short-coherence digital microscopy by use of a lensless holographic imaging system," Appl. Opt. **41,** 4489–4496 (2002).
15. E. Cuche, P. Marquet, and C. Depeursinge, "Spatial filtering for zero-order and twin-image elimination in digital off-axis holography," Appl. Opt. **39,** 4070–4075 (2000).
16. E. Cuche, P. Marquet, and C. Depeursinge, "Aperture apodization using cubic spline interpolation: application in digital holographic microscopy," Opt. Commun. **182,** 59–69 (2000).
17. E. Cuche, F. Bevilacqua, and C. Depeursinge, "Digital holography for quantitative phase-contrast imaging," Opt. Lett. **24,** 291–293 (1999).
18. E. Cuche, P. Marquet, and C. Depeursinge, "Simultaneous amplitude-contrast and quantitative phase-contrast microscopy by numerical reconstruction of Fresnel off-axis holograms," Appl. Opt. **38,** 6994–7001 (1999).
19. O. Camber, C. Rehbinder, T. Nikkila, and P. Edman, "Morphology of the pig cornea in normal conditions and after incubation in a perfusion apparatus," Acta Vet. Scand. **28,** 127–134 (1987).
20. K. Ludwig, E. Wegscheider, J. P. Hoops, and A. Kampik, "*In vivo* imaging of the human zonular apparatus with high-resolution ultrasound biomicroscopy," Arch. Ophtalmol. **237,** 361–371 (1999).
21. C. J. Pavlin and F. S. Foster, "High resolution ultrasound," in *Cornea*, J. H. Krachmer, M. J. Mannis, and E. J. Holland, eds. (Mosby, St. Louis, 1996), Chap. 21.